



## Third-order photon cross-correlations in resonance fluorescence

Yamil Nieves  and Andreas Muller\*

Physics Department, University of South Florida, Tampa, Florida 33620, USA

 (Received 14 August 2020; revised 5 October 2020; accepted 7 October 2020; published 19 October 2020)

We investigated third-order correlations between photons from a single quantum dot's resonance fluorescence in the strong excitation regime originating from opposite sidebands of the power spectrum. The three-time correlation measurements for photons filtered using three independent Fabry-Perot etalons resulted in correlation maps with “antibunching” features as a consequence of correlations originating from the same sideband, and “bunching ridges” due to opposite sideband correlated photons.

DOI: [10.1103/PhysRevB.102.155418](https://doi.org/10.1103/PhysRevB.102.155418)

### I. INTRODUCTION

The ability to control the output of a light emitter, such as a single-photon source, is a key component in the development of quantum optical technologies [1]. With the discovery of positively correlated photons—photons arriving together in “bunches” at the detector—by Hanbury-Brown and Twiss in 1956 [2], photon correlations have become the main focus of quantum optics in the pursuit of an ever-growing range of quantum applications, such as quantum cryptography [3–6], quantum metrology [7–10], ghost imaging [11–13], and quantum teleportation [14–17].

For a broad range of quantum processes, including those involving multiparticle interactions [18], photon correlations have been a powerful investigative tool thanks to the increasing performance of detection systems [19]. The correlations between the detection time of subsequently emitted photons serve as the primary tool for characterizing the type of radiation emitted through light-matter interactions at the few or single quantum level. For instance, the first-order correlation function,  $g^{(1)}(t_1)$ , can be readily obtained interferometrically and its Fourier transform provides the spectral line shape of emission of the light source. Although a  $g^{(1)}(t_1)$  measurement provides invaluable information about the light and the mechanism involving its generation, alone it reveals little about the source itself. For example, the  $g^{(1)}(t_1)$  spectral line shape from light originating from an ensemble of noninteracting radiating atoms is identical to that of a light source consisting of a single radiating atom (single-photon source). To distinguish the two, a second-order photon correlation measurement is required.

Under moderate photon flux, typical of continuous-wave experiments, the second-order correlation function,  $g^{(2)}(\tau)$ , is proportional to the histogram of the difference between the photon arrival times of two detection channels,  $\tau = t_2 - t_1$ . For a classical coherent light source (such as a laser) photons arrive at the detectors randomly with no mutual correlations and exhibit Poissonian statistics with  $g^{(2)}(\tau) \approx 1$ . Photons originating from an incoherent light source, e.g., a black body,

have the tendency to arrive in bunches at the detectors and are characterized by a peak within a short time-delay interval such that  $g^{(2)}(0) > 1$ . On the other hand, a typical quantum system—two-level systems such as a single radiating atom or quantum dot—uniquely exhibits a dip due to photon antibunching, i.e.,  $g^{(2)}(0) < 1$ , meaning that photons never arrive at the same time at the detectors.  $g^{(2)}(\tau)$  has been used extensively in the past decades to characterize a variety of light sources [20–25].

Correlation measurements beyond the second order have gained increased interest since early work using a streak camera revealed strong photon bunching statistics in third-order correlation measurements of microcavity laser light [26,27]. It was shown that the third-order correlation function,  $g^{(3)}(t_1, t_2, t_3)$ , provides more refined information about nonclassical light sources such as multiphoton differentiation [28] and the ability to analyze components [29]. Most recently, the nonclassical character of light emitted by a strongly coupled quantum dot–cavity system has been demonstrated up to fourth order [30]. However, while photon correlations have largely been scrutinized for their temporal character alone, other aspects, such as photon “indistinguishability,” are also tied to spectral properties of the light.

In the pursuit of quantum sources capable of emitting a bundle of  $N$  photons [31], there have been fascinating developments in the understanding of photon statistics with the generalization of *frequency-resolved* photon correlations which introduces the frequency aspect into the theory of photon correlations [32–34]. The  $N$ -photon spectrum is built on the notion of a time-dependent physical spectrum proposed by Eberly and Wódkiewicz [35], and of time-dependent correlation functions studied extensively by Knöll *et al.* [36]. The “ $N$ -photon spectrum,”  $g_{\Gamma_1, \dots, \Gamma_N}^{(N)}(t_1, \omega_1; \dots; t_N, \omega_N)$ , is proportional to the joint probability of detecting a photon at time  $t_1$  filtered at frequency  $\omega_1$  with a detector resolution (bandwidth)  $\Gamma_1, \dots$ , and a photon at time  $t_N$  filtered at frequency  $\omega_N$  with a bandwidth  $\Gamma_N$ . An interesting aspect of  $g_{\Gamma_1, \dots, \Gamma_N}^{(N)}(t_1, \omega_1; \dots; t_N, \omega_N)$  is that it reveals information about pathways underlying the generation of light in a given source [23]. Although the computation of such a function is challenging even at the second order [37], the pioneering

\*mullera@usf.edu

theoretical work of Del Valle *et al.* has introduced a method that allows one to compute this quantity without the approximations performed before, making calculations manageable even at high orders [38]. Recently, we provided validation of this method with experimental results of the frequency-resolved three-photon autocorrelation function  $g_{\Gamma_f}^{(3)}(\tau_1, \tau_2, \omega_f)$  [39] for the delays  $\tau_1 = t_2 - t_1$  and  $\tau_2 = t_3 - t_1$ .

Here we explore the third-order cross-correlation function which makes up the three-photon spectrum  $g_{\Gamma_1, \Gamma_2, \Gamma_3}^{(3)}(\tau_1, \tau_2; \omega_1, \omega_2, \omega_3)$  of single quantum dot (QD) resonance fluorescence under strong monochromatic laser illumination. Contrary to the autocorrelation measurements,  $g_{\Gamma_1, \Gamma_2, \Gamma_3}^{(3)}(\tau_1, \tau_2; \omega_1, \omega_2, \omega_3)$  involves three filters, each with independently tunable resonance frequencies.

In Sec. II, we provide background information on resonance fluorescence along with prior results summarized in the form of a third-order autocorrelation map. After describing the experimental setup in Sec. III, we report measurements of three-time cross-correlation maps in Sec. IV and provide a simple dressed-states interpretation. Finally, in Sec. V, we discuss notable experimental nonidealities including filter imperfections and spectral diffusion.

## II. BACKGROUND

A monochromatic laser interacting with a solid-state two-level system creates an electronic excitation which eventually relaxes radiatively to a ground state at a rate  $\kappa$ . *Resonance fluorescence* occurs when the driving laser's frequency,  $\omega_L$ , closely matches the natural frequency of the two-level system,  $\omega_0$ , which results in the generation of light via spontaneous emission at the same or very near the frequency of the laser. Under a sufficiently intense applied field (i.e., when  $\Omega \gg \kappa$ , where  $\Omega$  is the Rabi frequency characterizing the strength of the interaction), the line shape of the resonance fluorescence spectrum consists of three peaks centered at the laser frequency,  $\omega_L$ , commonly known as the ‘‘Mollow triplet’’ [40], where the side peaks are approximately separated from the central peak by  $\Omega$ . The origin of these peaks can be understood as a cascade down a ladder of dressed states, i.e., the eigenstates of the coupled light-matter Hamiltonian [41]. This power spectrum continues to be researched today, even in the semiclassical treatment [42], for its fascinating properties which may benefit emerging quantum information science applications [43]. Resonance fluorescence in the Mollow triplet regime serves as a unique platform for testing novel quantum optics concepts which have been extensively documented for isolated atoms [44], molecules [45], quantum dots [46–50], and Josephson junctions [51]. One such concept is the generalization of the ordinary spectrum to the  $N$ -photon spectrum.

In our previous work in Ref. [39], we reported the results of third-order autocorrelation measurements as shown in Fig. 1. Experimentally,  $g_{\Gamma_f}^{(1)}(\omega_f)$  can be measured by scanning the filter frequency and recording the count rates of one of the detectors. Figure 1(a) shows the filter configuration of each detection channel used to build the three-photon autocorrelation map in Fig. 1(b).

The correlation map in Fig. 1(b) was constructed by building a histogram of the time delays between the time tags of photons detected in channels 1 ( $t_2$ ) and 2 ( $t_3$ ) with respect to

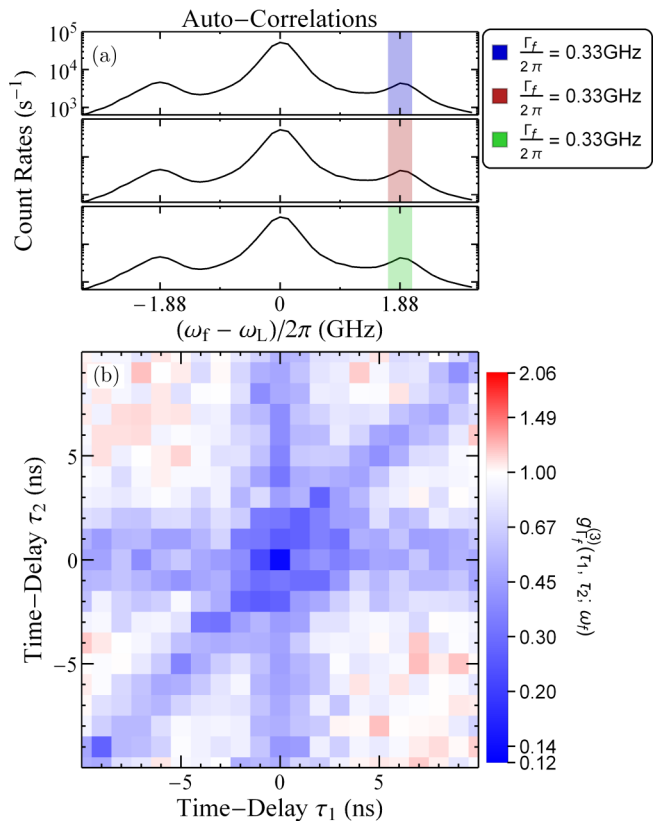


FIG. 1. (a) Filter configuration used to create the three-photon correlation map in (b) for time delays  $\tau_1 = t_2 - t_1$  and  $\tau_2 = t_3 - t_1$  where  $(\omega_f - \omega_L)/2\pi = \Omega/2\pi \approx 1.88$  GHz with a fixed filter bandwidth  $\Gamma_f/2\pi = 0.33$  GHz.

those detected in channel 0 ( $t_1$ ), that is,  $\tau_1 = t_2 - t_1$  and  $\tau_2 = t_3 - t_1$  within a 1 ns  $\times$  1 ns wide time bin. Figure 1(b) shows the three-photon autocorrelation map,  $g_{\Gamma_f}^{(3)}(\tau_1, \tau_2, \omega_f)$ , for photons originating from one of the Mollow triplet sidebands,  $(\omega_f - \omega_L) = \Omega$ , where photon antibunching is observed. The third-order correlation map reveals strong nonclassical coincidences at  $\tau_1 = \tau_2 = 0$  as well as two-photon antibunching troughs when only two out of three photons arrived at the detectors at the same time, that is, whenever  $\tau_1 = 0$  (vertical), when  $\tau_2 = 0$  (horizontal), and  $\tau_1 = \tau_2$  (diagonal). The objective of this work is to expand this investigation to include cross-correlation measurements for photons originating from different Mollow triplet spectral windows.

## III. EXPERIMENTAL SETUP

The  $N$ -photon correlations can be measured via a straightforward extension of a Hanbury-Brown and Twiss type measurement, wherein light from a source is split into  $N$  channels each equipped with a spectral filter and photon counting module. Here we probed molecular-beam-epitaxy-grown InAs QDs held in a cryostat (at base temperature of 4 K and strongly interacting with a resonant wave-guided monochromatic laser beam.

Our setup, depicted in Fig. 2, is optimized to minimize unwanted background laser scattering by using an orthogonal excitation/detection geometry where QDs were grown

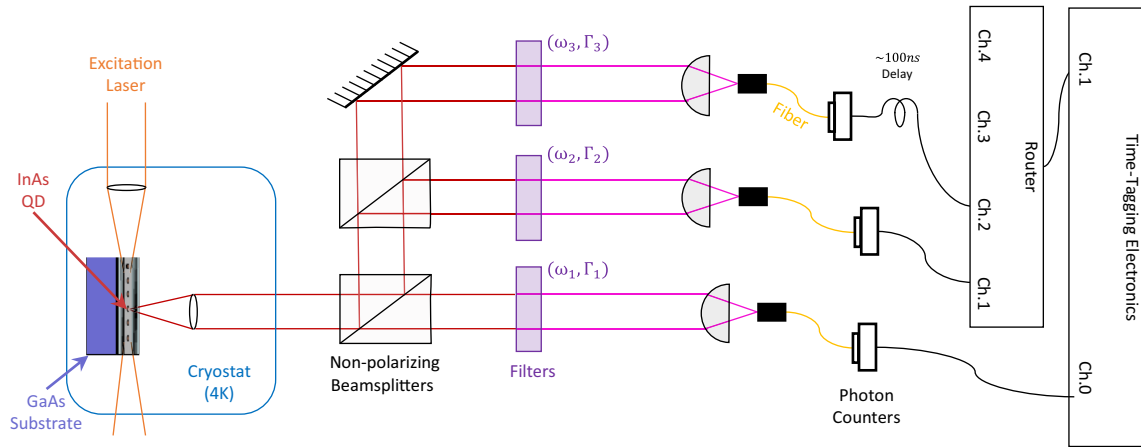


FIG. 2. Experimental setup: the light near-resonantly scattered by a strongly driven QD was collected and split three ways, with each path equipped with a spectral filter and photon counting module. Time-tagging of photon arrival times was performed on each channel independently.

between two distributed Bragg reflectors of moderate reflectivity [46]. The QD scattered light was split into three beams using two nonpolarizing beam splitters. Each beam passed through a thick solid Fabry-Perot etalon (reflectively coated silica cuboid), each with a free spectral range of 10 GHz. Each etalons' resonance frequency,  $\omega_f$ , was tuned independently by adjusting the cuboid's temperature to change the index of refraction of the etalon. For optimal heat distribution, the etalons were placed between two thermoelectric Peltier coolers [52] connected to temperature controllers (Thorlabs TED200C) managed remotely using a LABVIEW program. The bandwidth of each filter was fixed at  $\Gamma_1/2\pi = 500\text{MHz}$ ,  $\Gamma_2/2\pi = 750\text{MHz}$ , and  $\Gamma_3/2\pi = 670\text{MHz}$  by adjusting the incidence angle of the light entering the etalon.

After traversing the filters, the QD scattered light was detected by single-photon counting modules (Excelitas SPCM-AQRH-14). Tagging of photon arrival times was performed for each detection channel independently using time-tagging electronics (PicoQuant PicoHarp 300) at an overall detector-limited resolution of about 400 ps. As a replacement for a more expensive multichannel system, time-tagging for three channels was performed with the help of a router (PicoQuant PHR 800), where a 100 ns delay in electrical wiring was introduced to avoid the router's dead-time window. This delay was later removed during postprocessing.

#### IV. CROSS-CORRELATION MEASUREMENTS

As with the autocorrelation measurements in Fig. 1, cross-correlation maps were recorded by creating a histogram of photon arrival times from each channel, only this time for a set of configurations from filter frequencies  $(\omega_1, \omega_2, \omega_3)$ . The three-photon cross-correlation maps are shown at the bottom of Fig. 3 where the color code is chosen so that the antibunching statistics ( $g^{(3)} < 1$ ) are shown in blue, the classical correlations ( $g^{(3)} \approx 1$ ) in white, and the bunching statistics ( $g^{(3)} > 1$ ) are indicated in red.

Experimentally, we obtained  $g_{\Gamma_1\Gamma_2\Gamma_3}^{(3)}(\tau_1, \tau_2; \omega_1, \omega_2, \omega_3)$  by measuring the total coincidences at  $\tau_1$  and  $\tau_2$  (i.e., count of simultaneous detections) and normalizing by the total of

accidentals in the same time bin (i.e., the coincidences between a time-delay interval within which detections are uncorrelated; for example, the average of the total coincidences in a region in which  $\tau_1 = -\tau_2$  away from  $\tau_1 = \tau_2 = 0$ ):

$$g_{\Gamma_1, \Gamma_2, \Gamma_3}^{(3)}(\tau_1, \tau_2; \omega_1, \omega_2, \omega_3) = \frac{\text{Coincidences at } \tau_1, \tau_2}{\text{Accidentals}}.$$

The spectral line shapes above the correlation maps in Fig. 3 show the filter frequency configuration used for each correlation map relative to the power spectrum, wherein the resonance frequency of one filter is set to match one of the sidebands of the Mollow triplet while the other two filters are set to match the opposite sideband.

In contrast to the autocorrelation map in Fig. 1, only the antibunching troughs from the two autocorrelated filters remain, that is, the diagonal  $\tau_1 = \tau_2$  in Fig. 3(a), the horizontal at  $\tau_2 = 0$  in Fig. 3(b), and the vertical at  $\tau_1 = 0$  in Fig. 3(c). Meanwhile, the remaining troughs have now become coincidence ridges due to two-photon bunching from the cross-correlated photons. Furthermore it can be seen that the nonclassical character at  $\tau_1 = \tau_2 = 0$  in the autocorrelation map (Fig. 1), has turned into Poissonian statistics due to the superposition of second-order autocorrelated and second-order cross-correlated photons. Table I provides a quantitative comparison of the third corresponding to the central feature from each correlation map and second-order correlations between filters at zero time delay.

The origin of the features in the cross-correlation maps can be best visualized using the dressed states formalism, wherein the cascade down the ladder of superposition states that result from the diagonalization of the coupled QD-laser Hamiltonian can be used to describe the resonance fluorescence process [41]. In the dressed-states picture shown in Fig. 4, each two-state manifold is separated by the driving laser frequency,  $\omega_L$ , while the upper  $|+\rangle$  and lower  $|-\rangle$  states in the manifold are separated approximately by the Rabi frequency,  $\Omega$ . The resonance fluorescence process originating from the "long" sideband,  $\omega_L + \Omega$ , can be viewed as a transition from the upper state of a top manifold to the lower state

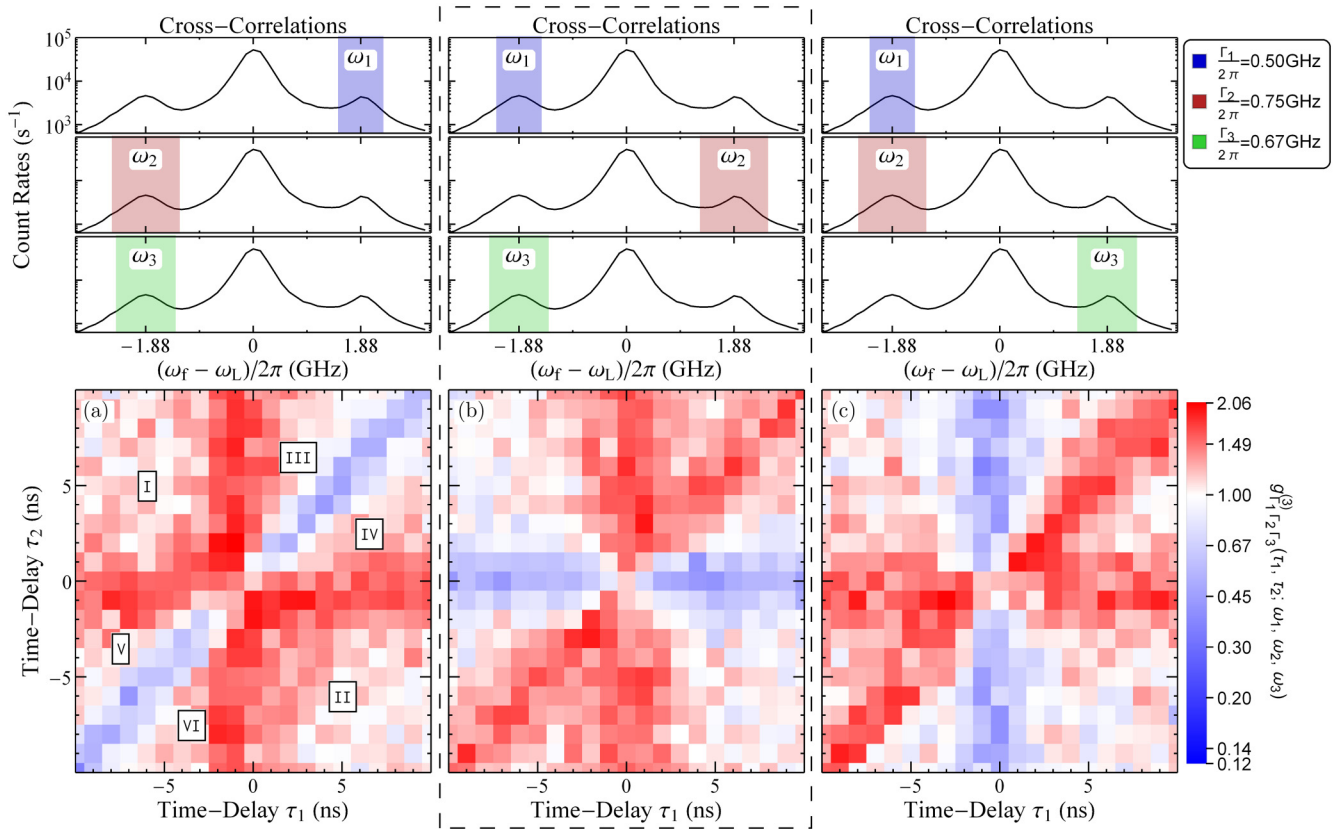


FIG. 3. Experimental three-photon correlation maps as a function of time delays  $\tau_1 = t_2 - t_1$  and  $\tau_2 = t_3 - t_1$  with fixed Rabi frequency of  $\Omega/2\pi \approx 1.88$  GHz for different filtering frequency configurations with filter bandwidths of  $\Gamma_1/2\pi = 0.5$  GHz,  $\Gamma_2/2\pi = 0.75$  GHz, and  $\Gamma_3/2\pi = 0.67$  GHz. Numerals in (a) show areas with different permutations of a fixed order of photon detection events (e.g., quadrant I includes detection events for which  $t_2 < t_1 < t_3$ ).

of a bottom manifold,  $|+\rangle \rightarrow |-\rangle$ . Meanwhile the photons originating from the “short” sideband,  $\omega_L - \Omega$ , occur due to the transitions from the lower state of a top manifold to the upper state of a bottom manifold,  $|-\rangle \rightarrow |+\rangle$ . The two- and three-photon emission can then be visualized as a cascade down this ladder as illustrated in Fig. 4.

The two-photon cascade from cross-correlated transitions accounts for the bunching that occurs due to connected transitions between states. On the other hand, disconnected pathways, and thus photon antibunching, are associated with the two-photon cascade from autocorrelated transitions, i.e., second-order events involving photons from the same sideband. The three-photon correlations become a superposition of all three possible cascades composed of a combination of disconnected and connected pathways.

## V. DISCUSSION

To better understand the experimental maps presented here, we may divide them into six regions corresponding to a fixed order of photon detection events as illustrated in Fig. 3(a). For example, the quadrant I (at the upper-left corner) corresponds to a photon detection order  $t_2 < t_1 < t_3$ , meaning that a photon from channel 2 is detected first, followed by a photon detected in channel 1, and the last photon detected will result from channel 3. Meanwhile, the quadrant II (at the lower-right corner) corresponds to a channel detection order for which  $t_3 < t_1 < t_2$ , meaning a photon in channel 3 is detected first, followed by a photon in channel 1, and then by a photon from channel 2. The remaining octants at the top-right and bottom-left corners correspond to remaining orders of channel

TABLE I. Raw data for each correlation map showing the total recording time, the total third-order coincidences at  $\tau_1 = \tau_2 = 0$ , the total of accidentals obtained from the average coincidences around an antidiagonal away from zero for a  $1 \text{ ns} \times 1 \text{ ns}$  time bin, and the normalized third- and second-order correlations at  $\tau_1 = \tau_2 = 0$ .

Figure	Exposure time (s)	Third-order coincidences	Third-order accidentals	$g^{(3)}(0; \omega_1, \omega_2, \omega_3)$	$g^{(2)}(0; \omega_1, \omega_2)$	$g^{(2)}(0; \omega_1, \omega_3)$	$g^{(2)}(0; \omega_2, \omega_3)$
1	190 083	10	77.65	$0.13 \pm 0.04$	0.50	0.50	0.49
3(a)	526 193	84	73.85	$1.14 \pm 0.08$	1.46	1.51	0.51
3(b)	562 604	86	75.30	$1.14 \pm 0.14$	1.51	0.48	1.48
3(c)	354 181	58	47.50	$1.22 \pm 0.13$	0.48	1.47	1.60



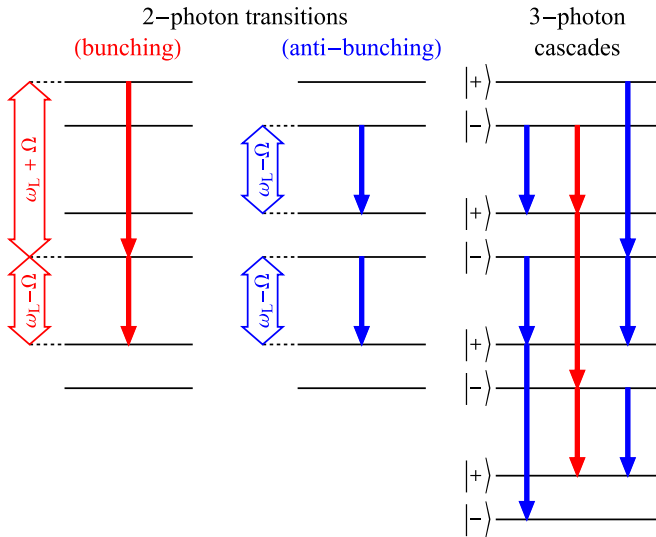


FIG. 4. Dressed-states picture illustrating the origin of the features in Fig. 3. The bunching statistics due to connected emission pathways from second-order cross-correlated photons correspond to the vertical ( $\tau_1 = 0$ ) and horizontal ( $\tau_2 = 0$ ) features in Fig. 3(a), the diagonal ( $\tau_1 = \tau_2$ ) and vertical in Fig. 3(b), and the diagonal and horizontal in Fig. 3(c). On the other hand, the antibunching statistics due to disconnected emission pathways from the second-order autocorrelated photons correspond to the diagonal in Fig. 3(a), the horizontal in Fig. 3(b), and the vertical in Fig. 3(c). Meanwhile, the superposition of the three-photon cascades corresponds to the central feature of all correlation maps in Fig. 3.

detection events  $t_1 < t_2 < t_3$  for octant III,  $t_1 < t_3 < t_2$  for octant IV,  $t_3 < t_2 < t_1$  for octant V, and  $t_2 < t_3 < t_1$  for octant VI. This order is the same for all correlation maps shown here.

The locations of interest, however, are at the boundaries between each region, at which two out of three photons are detected simultaneously, or right at the center of the map at  $\tau_1 = \tau_2 = 0$ , at which all three photons are detected at the same time. At these boundaries, the presence of bunching or antibunching depends on whether it corresponds to emission from alternating sidebands, or if the emission process involves consecutive emission from the same sideband. The central features at  $\tau_1 = \tau_2 = 0$  of the experimental maps constitute a small subset of the data required to reconstruct the complete three-photon spectrum of single QD resonance fluorescence. Specifically, by repeating such measurements for a matrix of frequency triplets  $(\omega_1, \omega_2, \omega_3)$  and logging the normalized coincidence rate, an entire  $g_{\Gamma_1, \Gamma_2, \Gamma_3}^{(3)}(0, 0; \omega_1, \omega_2, \omega_3)$  coincidence “cube” would be obtained. It is worth mentioning these measurements are not specific to quantum dots, but rather are a characteristic of the resonance fluorescence of a two-level system.

In practice, however, many hurdles remain before such a quantity can be measured. An obvious obstacle is the impractically long recording times that would be required (Table I). This limitation could at least in part be remedied by improving the collection and propagation efficiency, as well as the detector quantum efficiency in our experiments, or by using more complex approaches, for instance those which employ photonic nanowires [53], microlenses [54], broadband

enhancement solutions using bullseye structures [55], or in general make use of the Purcell effect of cavity quantum electrodynamics [56].

Another complication that may introduce nonidealities is the stabilization and uniformity of the properties of the spectral filters. For instance, the filter resonance frequencies will inevitably fluctuate during the measurement as will the filter bandwidth. In addition, the precise width of each spectral filter may be difficult to set to an arbitrary independent value, and to maintain over time. In the measurements presented here, the filters had slightly different bandwidths, which explains in part the variations between the three panels. Were it not for slightly different properties of individual filters the three configurations would be equivalent to those obtained by simply switching electric cables between detectors and time-tagging electronics.

Small variations in filter bandwidths are particularly consequential when the filter bandwidth is near the natural linewidth of the emitter. In fact it was recently shown that, even in the weak excitation regime, the photon statistics of a filtered single QD’s resonance fluorescence depend dramatically on the filter bandwidth [57].

Lastly, the transition frequency of the QD being probed will fluctuate to some extent. This “spectral diffusion” results in inhomogeneous broadening, i.e., an averaging over different QD resonance frequencies. To examine the consequences of spectral diffusion under various filter bandwidths, we turn to theoretical simulations of the power spectrum (the “one-photon spectrum”) given explicitly by [40,58]

$$g_{\Gamma_f}^{(1)}(\omega_f) = 2\text{Re} \left\{ \left[ \left( i(\omega_L - \omega_f) + \frac{\Gamma_f}{2} \right) \mathbb{1} - \mathbb{M} \right]_{(2,2)}^{-1} n_\infty + \left[ \left( i(\omega_L - \omega_f) + \frac{\Gamma_f}{2} \right) \mathbb{1} - \mathbb{M} \right]_{(2,4)}^{-1} \alpha_\infty^* \right\}, \quad (1)$$

where  $\mathbb{1}$  is the  $4 \times 4$  identity matrix, and  $[\dots]_{(i,j)}$  denotes the element  $(i, j)$  of the resulting matrix. The expression for the steady-state probability of finding the two-level system in its excited state  $n_\infty$ , the quantum-mechanical expectation value of the two-level coherence  $\alpha_\infty$ , and the matrix  $\mathbb{M}$  capturing the inputs of the equation of motion for the system’s observables are given by

$$n_\infty = \frac{\Omega^2}{\kappa} \left( \frac{\kappa + 2\gamma}{4\Delta^2 + (\kappa + 2\gamma)(\kappa + 2\gamma + 2\Omega^2/\kappa)} \right),$$

$$\alpha_\infty = i\Omega \left( \frac{\kappa + 2\gamma + 2i\Delta}{4\Delta^2 + (\kappa + 2\gamma)(\kappa + 2\gamma + 2\Omega^2/\kappa)} \right),$$

and

$$\mathbb{M} = \begin{pmatrix} -\kappa & -i\frac{\Omega}{2} & i\frac{\Omega}{2} & 0 \\ -i\frac{\Omega}{2} & -\frac{\kappa}{2} - \gamma + i\Delta & 0 & i\frac{\Omega}{2} \\ i\frac{\Omega}{2} & 0 & -\frac{\kappa}{2} - \frac{\gamma}{2} - i\Delta & -i\frac{\Omega}{2} \\ \kappa & i\frac{\Omega}{2} & -i\frac{\Omega}{2} & 0 \end{pmatrix},$$

where  $\Delta = \omega_0 - \omega_L$  is the detuning between the QD resonance frequency and the laser frequency. At the temperature of 4 K at which measurements were performed pure dephasing is known to not play a major role in the spectral broadening of InAs QD excitonic transitions [58], thus, for simplicity, here

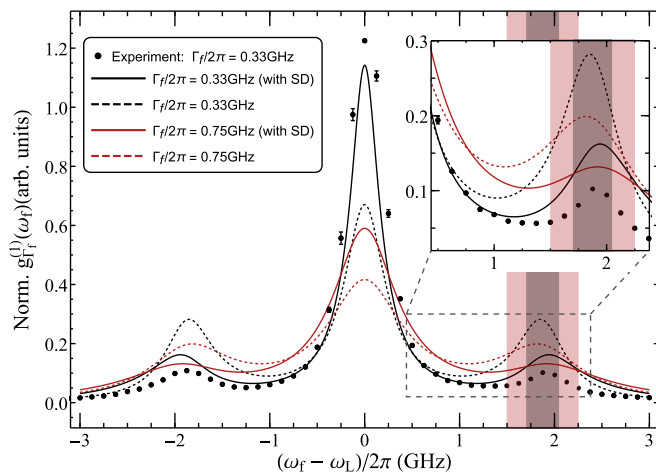


FIG. 5. Experimental and theoretical Mollow triplet line shape with Rabi frequency  $\Omega/2\pi = 1.88$  GHz for filter bandwidths  $\Gamma_f/2\pi = 0.33$  GHz (black) and  $\Gamma_f/2\pi = 0.75$  GHz (red). Theoretical traces with (solid) and without (dashed) spectral diffusion (SD) are based on Eqs. (2) and (1), respectively, with a radiative decay rate  $\kappa/2\pi = 0.2$  GHz, and a pure dephasing rate  $\gamma = 0$ .

we assume no pure dephasing, i.e.,  $\gamma = 0$ . Furthermore, we assume a radiative decay rate  $\kappa/2\pi = 0.2$  GHz, consistent with a typical radiative lifetime of  $\tau_r = 1/(2\pi\kappa) = 1$  ns for InAs QDs [59]. Phonon scattering has been ignored even though its effect is measurable albeit over a significantly broader spectral range than the one of interest here [58]. To capture the effects of individual dephasing processes on the correlation functions would actually require reducing the detection resolution which in our measurements is dominated by the 1 ns time bin width.

To account for the fluctuations of the QD resonance frequency,  $\omega_0$ , due to spectral diffusion [60,61], as in Ref. [58], we assume a Gaussian distribution of the detuning between the QD resonance frequency and the laser frequency,  $\Delta$  (centered at  $\Delta_\mu = 0$  with a standard deviation  $\Delta_\sigma = 2$  GHz), and integrating Eq. (1) over all possible random detunings:

$$\tilde{g}_{\Gamma_f}^{(1)}(\omega_f) \propto \int g_{\Gamma_f}^{(1)}(\omega_f, \Delta) e^{-(\Delta - \Delta_\mu)^2 / 2\Delta_\sigma^2} d\Delta. \quad (2)$$

Figure 5 shows the normalized power spectrum obtained experimentally by scanning a filter with bandwidth  $\Gamma_f/2\pi = 0.33$  GHz, and the theoretical simulations for  $\tilde{g}_{\Gamma_f}^{(1)}(\omega_f)$  using the same bandwidth as the experimental trace, and for  $\Gamma_f/2\pi = 0.75$  GHz which matches the largest bandwidth

involved in the cross-correlation maps in Fig. 3. The theoretical power spectrum in the absence of spectral diffusion, obtained directly using Eq. (1), is also included.

From Fig. 5 it is clear that spectral diffusion substantially impacts the measured correlations. In particular, it leads to a greater central peak magnitude relative to the sideband magnitude compared to the case of a purely radiatively broadened two-level system. In that sense spectral diffusion causes an effectively reduced interaction strength since, during part of the measurement, the laser is off-resonance with the QD.

In addition, Fig. 5 reveals how a larger filter bandwidth increases the spectral overlap between the central peak tails and the sidebands, even more so in the presence of spectral diffusion. This source of ‘‘contamination’’ may be in principle avoided by increasing the Rabi frequency, which was not possible in our current experimental configuration. Altogether, variations over time in the QD resonance frequency and in the filter properties reduce the degree of bunching and the degree of antibunching in the maps of Fig. 3. In principle, such effects could all be captured by an extension of the theory of Ref. [38], and a quantitative theory/experiment comparison could be made, even at third order with independent filter frequencies.

## VI. CONCLUSION

In summary, spectrally filtered third-order photon cross-correlations were recorded for resonance fluorescence from an individual semiconductor quantum dot under strong laser illumination. Previous results reported in Ref. [39] correspond to only a single point in the third-order spectral correlation space. In this work, we presented considerably more challenging measurements involving three separate filter configurations, namely, those for which the resonance frequency of two of the filters matches the lower frequency sideband of the Mollow triplet, while the remaining filter is set at the opposite sideband. The resulting correlation maps provide a stepping-stone towards constructing a complete three-photon spectrum. Furthermore, the revelation of a rich landscape of bunching and antibunching features opens the way for potential new quantum devices capable of producing two-photon bunching or antibunching on demand. Additionally, our measurements highlight how, in practice, these measurements are sensitive to filter bandwidths and spectral fluctuations of the QD resonance frequency over time. Future progress will likely hinge upon technical filter improvements and operation at higher Rabi frequency. A complete three-photon spectrum may be mapped for quantum dot resonance fluorescence, but also any other light source, so long as photon emission rates are large enough.

[1] T. D. Ladd, F. Jelezko, R. Laflamme, Y. Nakamura, C. Monroe, and J. L. O’Brien, *Nature (London)* **464**, 45 (2010).  
 [2] R. H. Brown and R. Q. Twiss, *Nature (London)* **177**, 27 (1956).  
 [3] A. K. Ekert, *Phys. Rev. Lett.* **67**, 661 (1991).  
 [4] W. T. Buttler, R. J. Hughes, P. G. Kwiat, S. K. Lamoreaux, G. G. Luther, G. L. Morgan, J. E. Nordholt, C. G. Peterson, and C. M. Simmons, *Phys. Rev. Lett.* **81**, 3283 (1998).

[5] W. Tittel, J. Brendel, H. Zbinden, and N. Gisin, *Phys. Rev. Lett.* **81**, 3563 (1998).  
 [6] A. Soujaeff, T. Nishioka, T. Hasegawa, S. Takeuchi, T. Tsurumaru, K. Sasaki, and M. Matsui, *Opt. Express* **15**, 726 (2007).  
 [7] V. Giovannetti, S. Lloyd, and L. Maccone, *Phys. Rev. Lett.* **96**, 010401 (2006).

- [8] J. Joo, W. J. Munro, and T. P. Spiller, *Phys. Rev. Lett.* **107**, 083601 (2011).
- [9] G. Tóth and I. Apellaniz, *J. Phys. A: Math. Theor.* **47**, 424006 (2014).
- [10] W. Dür, M. Skotiniotis, F. Fröwis, and B. Kraus, *Phys. Rev. Lett.* **112**, 080801 (2014).
- [11] T. B. Pittman, Y. H. Shih, D. V. Strekalov, and A. V. Sergienko, *Phys. Rev. A* **52**, R3429(R) (1995).
- [12] D. V. Strekalov, A. V. Sergienko, D. N. Klyshko, and Y. H. Shih, *Phys. Rev. Lett.* **74**, 3600 (1995).
- [13] C. H. Monken, P. H. Souto Ribeiro, and S. Pádua, *Phys. Rev. A* **57**, 3123 (1998).
- [14] D. Bouwmeester, J.-W. Pan, K. Mattle, M. Eibl, H. Weinfurter, and A. Zeilinger, *Nature (London)* **390**, 575 (1997).
- [15] D. Boschi, S. Branca, F. De Martini, L. Hardy, and S. Popescu, *Phys. Rev. Lett.* **80**, 1121 (1998).
- [16] M. Riebe, H. Häffner, C. Roos, W. Hänsel, J. Benhelm, G. Lancaster, T. Körber, C. Becher, F. Schmidt-Kaler, D. James *et al.*, *Nature (London)* **429**, 734 (2004).
- [17] T. Müller, M. Anderson, J. Huwer, J. Skiba-Szymanska, A. B. Krysa, R. M. Stevenson, J. Heffernan, D. A. Ritchie, and A. J. Shields, in *Quantum Information and Measurement* (Optical Society of America, Washington, DC, 2019), pp. S2A–S24.
- [18] S. Bounouar, M. Strauß, A. Carmele, P. Schnauber, A. Thoma, M. Gschrey, J.-H. Schulze, A. Strittmatter, S. Rodt, A. Knorr, and S. Reitzenstein, *Phys. Rev. Lett.* **118**, 233601 (2017).
- [19] E. Schlottmann, M. von Helversen, H. A. M. Leymann, T. Lettau, F. Krüger, M. Schmidt, C. Schneider, M. Kamp, S. Höfling, J. Beyer, J. Wiersig, and S. Reitzenstein, *Phys. Rev. Applied* **9**, 064030 (2018).
- [20] A. Aspect, G. Roger, S. Reynaud, J. Dalibard, and C. Cohen-Tannoudji, *Phys. Rev. Lett.* **45**, 617 (1980).
- [21] C. A. Schrama, G. Nienhuis, H. A. Dijkerman, C. Steijsiger, and H. G. M. Heideman, *Phys. Rev. A* **45**, 8045 (1992).
- [22] P. Michler, A. Kiraz, C. Becher, W. Schoenfeld, P. Petroff, L. Zhang, E. Hu, and A. Imamoglu, *Science* **290**, 2282 (2000).
- [23] A. González-Tudela, F. P. Laussy, C. Tejedor, M. J. Hartmann, and E. del Valle, *New J. Phys.* **15**, 033036 (2013).
- [24] M. Peiris, B. Petrak, K. Konthasinghe, Y. Yu, Z. C. Niu, and A. Muller, *Phys. Rev. B* **91**, 195125 (2015).
- [25] V. N. Shatokhin and S. Y. Kilin, *Phys. Rev. A* **94**, 033835 (2016).
- [26] J. Wiersig, C. Gies, F. Jahnke, M. Aßmann, T. Berstermann, M. Bayer, C. Kistner, S. Reitzenstein, C. Schneider, S. Höfling, A. Forchel, C. Kruse, J. Kalden, and D. Hommel, *Nature (London)* **460**, 245 (2009).
- [27] M. Aßmann, F. Veit, M. Bayer, M. van der Poel, and J. M. Hvam, *Science* **325**, 297 (2009).
- [28] D. Elvira, X. Hachair, V. B. Verma, R. Braive, G. Beaudoin, I. Robert-Philip, I. Sagnes, B. Baek, S. W. Nam, E. A. Dauler, I. Abram, M. J. Stevens, and A. Beveratos, *Phys. Rev. A* **84**, 061802(R) (2011).
- [29] M. J. Stevens, S. Glancy, S. W. Nam, and R. P. Mirin, *Opt. Express* **22**, 3244 (2014).
- [30] A. Rundquist, M. Bajcsy, A. Majumdar, T. Sarmiento, K. Fischer, K. G. Lagoudakis, S. Buckley, A. Y. Piggott, and J. Vučković, *Phys. Rev. A* **90**, 023846 (2014).
- [31] C. Sánchez Muñoz, E. del Valle, A. González Tudela, K. Müller, S. Lichtmanecker, M. Kaniber, C. Tejedor, J. J. Finley, and F. P. Laussy, *Nat. Photonics* **8**, 550 (2014).
- [32] L. Knöll and G. Weber, *J. Phys. B: At. Mol. Phys.* **19**, 2817 (1986).
- [33] J. Cresser, *J. Phys. B: At. Mol. Phys.* **20**, 4915 (1987).
- [34] L. Knöll, W. Vogel, and D.-G. Welsch, *Phys. Rev. A* **42**, 503 (1990).
- [35] J. H. Eberly and K. Wódkiewicz, *J. Opt. Soc. Am.* **67**, 1252 (1977).
- [36] L. Knöll, G. Weber, and T. Schafer, *J. Phys. B: At. Mol. Phys.* **17**, 4861 (1984).
- [37] R. Centeno Neelen, D. M. Boersma, M. P. van Exter, G. Nienhuis, and J. P. Woerdman, *Opt. Commun.* **100**, 289 (1993).
- [38] E. del Valle, A. González-Tudela, F. P. Laussy, C. Tejedor, and M. J. Hartmann, *Phys. Rev. Lett.* **109**, 183601 (2012).
- [39] Y. Nieves and A. Muller, *Phys. Rev. B* **98**, 165432 (2018).
- [40] B. R. Mollow, *Phys. Rev.* **188**, 1969 (1969).
- [41] C. Cohen-Tannoudji and S. Reynaud, *Philos. Trans. R. Soc. London A* **293**, 223 (1979).
- [42] H.-T. Chen, T. E. Li, A. Nitzan, and J. E. Subotnik, *J. Phys. Chem. Lett.* **10**, 1331 (2019).
- [43] H. J. Kimble, *Nature (London)* **453**, 1023 (2008).
- [44] F. Schuda, C. R. Stroud, Jr., and M. Hercher, *J. Phys. B: At. Mol. Phys.* **7**, L198 (1974).
- [45] G. Wrigge, I. Gerhardt, J. Hwang, G. Zumofen, and V. Sandoghdar, *Nat. Phys.* **4**, 60 (2008).
- [46] A. Muller, E. B. Flagg, P. Bianucci, X. Y. Wang, D. G. Deppe, W. Ma, J. Zhang, G. J. Salamo, M. Xiao, and C. K. Shih, *Phys. Rev. Lett.* **99**, 187402 (2007).
- [47] X. Xu, B. Sun, P. R. Berman, D. G. Steel, A. S. Bracker, D. Gammon, and L. J. Sham, *Science* **317**, 929 (2007).
- [48] E. B. Flagg, A. Muller, J. W. Robertson, S. Founta, D. G. Deppe, M. Xiao, W. Ma, G. J. Salamo, and C. K. Shih, *Nat. Phys.* **5**, 203 (2009).
- [49] S. M. Ulrich, S. Ates, S. Reitzenstein, A. Löffler, A. Forchel, and P. Michler, *Phys. Rev. Lett.* **106**, 247402 (2011).
- [50] C. Roy and S. Hughes, *Phys. Rev. Lett.* **106**, 247403 (2011).
- [51] O. Astafiev, A. M. Zagoskin, A. A. Abdumalikov, Jr., Y. A. Pashkin, T. Yamamoto, K. Inomata, Y. Nakamura, and J. S. Tsai, *Science* **327**, 840 (2010).
- [52] B. Petrak, M. Peiris, and A. Muller, *Rev. Sci. Instrum.* **86**, 023104 (2015).
- [53] J. Claudon, J. Bleuse, N. S. Malik, M. Bazin, P. Jaffrennou, N. Gregersen, C. Sauvan, P. Lalanne, and J.-M. Gérard, *Nat. Photonics* **4**, 174 (2010).
- [54] M. Gschrey, A. Thoma, P. Schnauber, M. Seifried, R. Schmidt, B. Wohlfeil, L. Krüger, J.-H. Schulze, T. Heindel, S. Burger *et al.*, *Nat. Commun.* **6**, 7662 (2015).
- [55] L. Sapienza, M. Davanço, A. Badolato, and K. Srinivasan, *Nat. Commun.* **6**, 7833 (2015).
- [56] C. Sánchez Muñoz, F. P. Laussy, E. del Valle, C. Tejedor, and A. González-Tudela, *Optica* **5**, 14 (2018).

- [57] C. L. Phillips, A. J. Brash, D. P. S. McCutcheon, J. Iles-Smith, E. Clarke, B. Royall, M. S. Skolnick, A. M. Fox, and A. Nazir, *Phys. Rev. Lett.* **125**, 043603 (2020).
- [58] K. Konthasinghe, J. Walker, M. Peiris, C. K. Shih, Y. Yu, M. F. Li, J. F. He, L. J. Wang, H. Q. Ni, Z. C. Niu, and A. Muller, *Phys. Rev. B* **85**, 235315 (2012).
- [59] M. Colocci, A. Vinattieri, L. Lippi, F. Bogani, M. Rosa-Clot, S. Taddei, A. Bosacchi, S. Franchi, and P. Frigeri, *Appl. Phys. Lett.* **74**, 564 (1999).
- [60] M. Pelton, D. G. Grier, and P. Guyot-Sionnest, *Appl. Phys. Lett.* **85**, 819 (2004).
- [61] S. F. Lee and M. A. Osborne, *ChemPhysChem* **10**, 2174 (2009).